Agricultural and Forest Meteorology 230–231 (2016) 67–78

Contents lists available at ScienceDirect

Agricultural and Forest Meteorology

journal homepage: www.elsevier.com/locate/agrformet

High resolution surface radiation products for studies of regional energy, hydrologic and ecological processes over Heihe river basin, northwest China

Guanghui Huang[a,b,*], Xin Li[a,c], Mingguo Ma[d], Hongyi Li[a,b], Chunlin Huang[a,e]

[a] Key Laboratory of Remote Sensing of Gansu Province, CAREERI, CAS, Lanzhou 730000, China
[b] Cold and Arid Regions Remote Sensing Observation System Experimental Station, CAREERI, CAS, Lanzhou 730000, China
[c] CAS Center for Excellence in Tibetan Plateau Earth Sciences, Chinese Academy of Sciences, China
[d] Southwest University, No.2, Tiansheng Road, BeiBei District, Chongqing 400715, China
[e] Jiangsu Center for Collaborative Innovation in Geographical Information Resource Development and Application, Nanjing 210023, China

ARTICLE INFO

Article history:
Received 18 June 2015
Received in revised form 4 January 2016
Accepted 11 April 2016
Available online 18 April 2016

Keywords:
PAR
Solar radiation
Net radiation
Geostationary Meteorological Satellite
MODIS

ABSTRACT

This paper presents a framework to obtain high spatial resolution regional surface photosynthetically active radiation (PAR), solar radiation (SSR) and net radiation (NR) products through combining Geostationary Meteorological Satellite (GMS) data, polar-orbiting satellite Moderate Resolution Imaging Spectrometer (MODIS) products and ground meteorological sites' observations. Huang et al. (2011) approach was adopted and improved to directly retrieve instantaneous PAR and SSR from GMS data; while for NR the relationship between net radiation and net solar radiation was analyzed and calibrated using ground observations and Normalized Difference Vegetation Index (NDVI). Then these instantaneous estimates with temporal resolution of half hour would be averaged or integrated to acquire hourly and daytime accumulated PAR, SSR and NR. Taking Heihe river basin in northwest China, a typical oasis-desert area, as an example, the methodology was applied to produce year 2012 PAR, SSR and NR products. Ground measurements from Watershed Allied Telemetry Experimental Research (WATER, Li et al. (2009)) and Heihe Watershed Allied Telemetry Experimental Research (HiWATER, Li et al. (2013)) were used to perform the accuracy assessments. The results indicate highly reliable products at 1 km resolution have been produced over this basin, and are applicable to the researches of the regional surface energy, hydrological and ecological processes.

1. Introduction

Surface radiation budget (SRB) serves as a key driving force for many physical and biological processes such as evapotranspiration, photosynthesis, and heating of surface soil and air, and thus strongly affects land-atmosphere interaction, agricultural production, even the general atmospheric circulation pattern and the development of the planetary boundary-layer. Therefore, SRB and its components always are required by various applications including weather forecasting, climate monitoring and modelling, water resource planning and managing, as well as agricultural meteorology.

Currently, there are already some global and regional surface radiation data sets routinely produced and provided by different scientific groups and organizations. Famous ones include radiative flux profile data set provided by International Satellite Cloud Climatology Project (ISCCP-FD), surface and top-of-atmosphere (TOA) shortwave and longwave radiative fluxes produced by Global Energy and Water Exchanges Project (GEWEX-SRB), Clouds and the Earth's Radiant Energy System (CERES) TOA and surface fluxes data, and Global Land Surface Satellite (GLASS) shortwave radiation products (Huang et al., 2013; Liang et al., 2013; Wielicki et al., 1996; Zhang et al., 2013, 2004, 2006). However, the coarse spatial and temporal resolutions prevent these data sets from being further used in various complicated ecological, meteorological and hydrological researches and applications on watershed and even regional scales. Therefore, in this paper we present a framework of computing high resolutions surface photosynthetically active radiation (PAR), solar radiation (SSR) and net

* Corresponding author at: Cold and Arid Regions Environmental and Engineering Research Institute, Chinese Academy of Sciences, Lanzhou, 730000, China.
E-mail address: luckhgh@lzb.ac.cn (G. Huang).

http://dx.doi.org/10.1016/j.agrformet.2016.04.007
0168-1923/

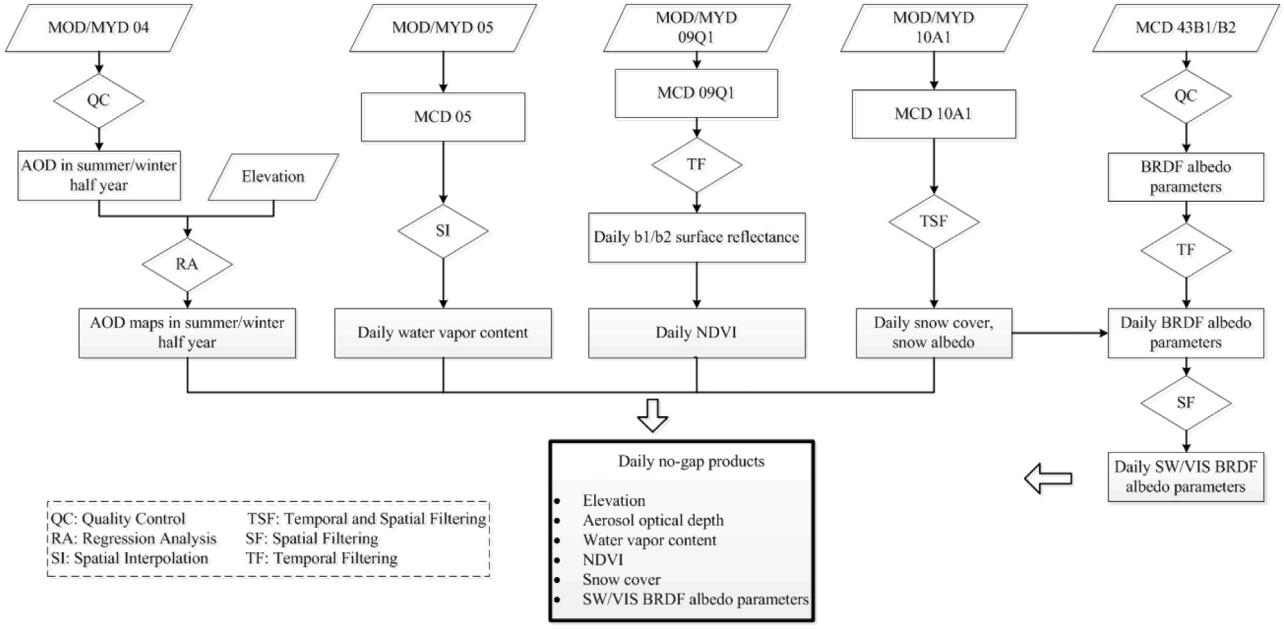

Fig. 1. Simplified flowchart of preparing surface and atmospheric state parameters required for estimating surface PAR, SSR and NR.

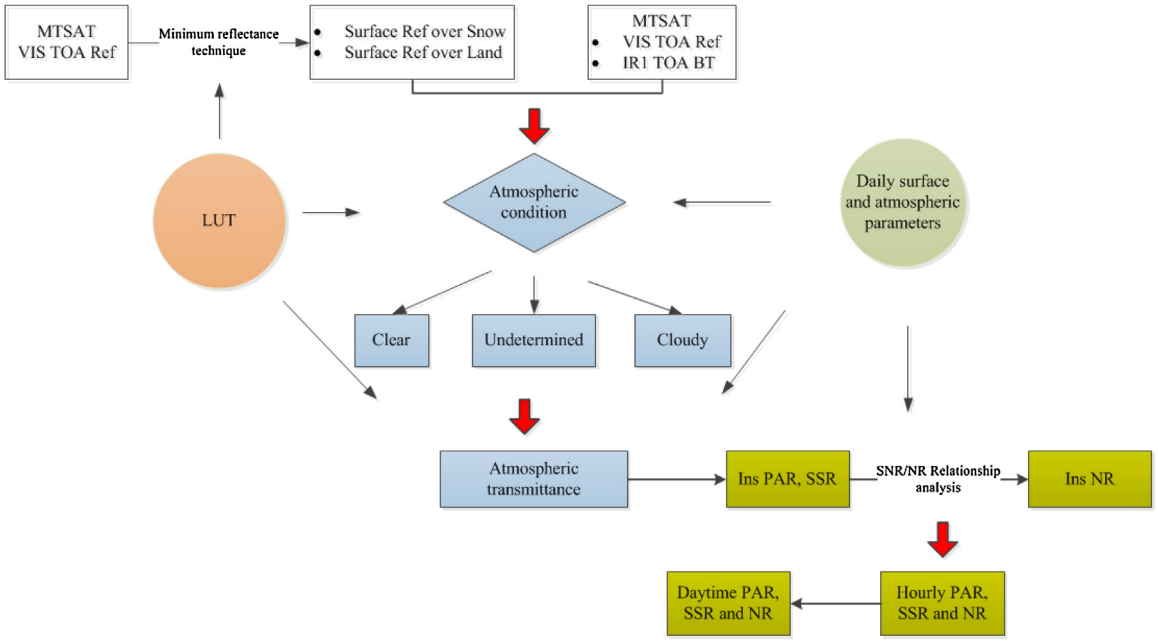

Fig. 2. Framework of estimating surface PAR, SSR and NR (instantaneous, hourly and daytime accumulated).

radiation (NR) and adopt it to produce the three main SRB component products in Heihe river basin, northwest China.

As primary SRB components, surface PAR and SSR had been explored and summarized in countless literatures, and many different types of approaches had been proposed from conventional meteorological parameterizations to retrieving algorithms based on satellite data (Deneke et al., 2008; Grant et al., 2004; Li et al., 2007; Liang et al., 2006; Liu et al., 2008; Lu et al., 2010; Pinker et al., 2007; Qin et al., 2011; Trnka et al., 2005; Yang and Koike, 2005; Zhang et al., 2006; Zheng et al., 2008). Due to being able to get rid of dependence on surface measurements, relatively complete spatial coverage and constantly appearances of new sophisticated satellite sensors, satellite remote sensing technique is playing a more important role in recent researches. A more detailed discussion on retrievals of PAR and SSR using satellite data had been summarized and given in our previous paper (Huang et al., 2011). Meanwhile, our previous research also demonstrated that considerable accuracy SSR could be estimated using the quantitative remote sensing technique by the synergy of geostationary meteorological satellite and polar-orbiting satellite over China. Therefore, in this study we still adopted the similar approach to estimate surface PAR and SSR, but some improvements had been imported to further polish the algorithm.

However, for the estimation of surface NR it is still very challengeable to only rely on satellite data, because not all of the components of SRB can be retrieved by satellite remote sensing technique. Conversely, the upward and downward longwave radiative fluxes are very difficult to accurately obtain from TOA

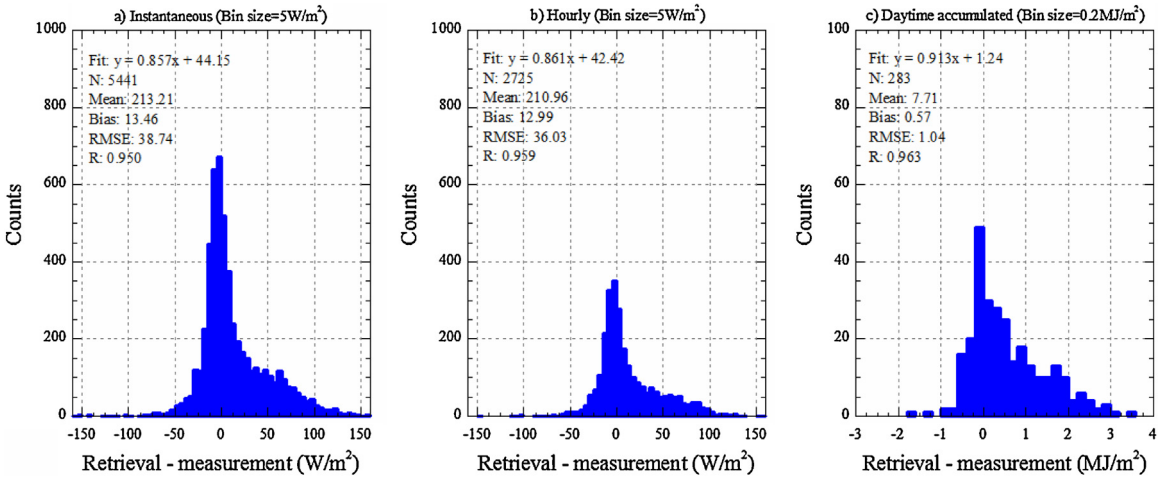

Fig. 3. Error histograms between the measured and estimated surface PAR at Daman site: (a) Instantaneous; (b) Hourly; (c) Daytime accumulated.

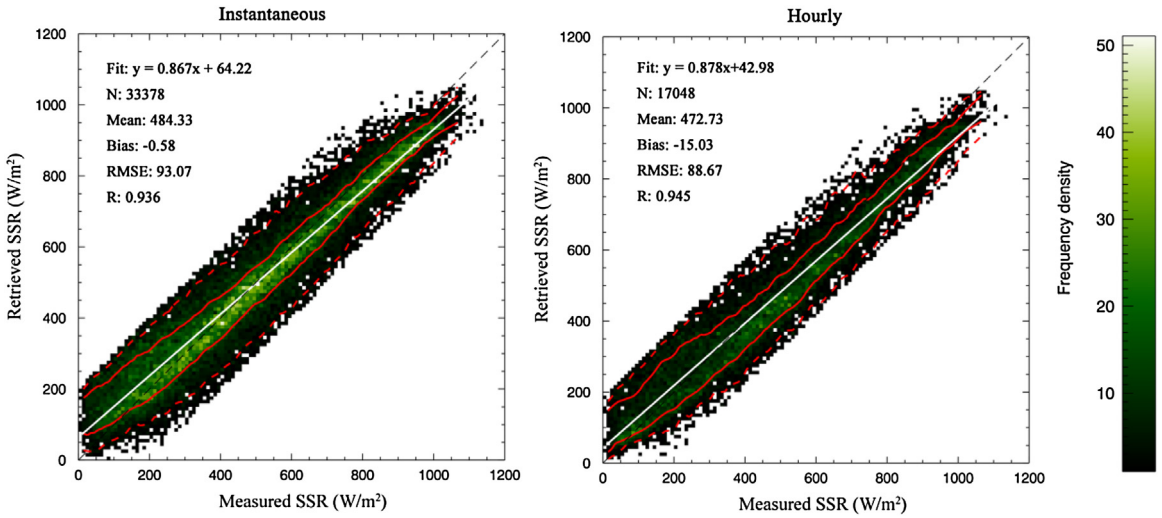

Fig. 4. Comparisons of the measured and retrieved instantaneous (left) and hourly (right) SSR. The region between two red solid lines encloses 66% of the retrievals for a given measured value, while that between two red dash lines is 95%. The white and black dash lines are the fitted line and the 1-1 line, respectively. The color represents the number density and only the number density >2 is shown in the figure. (For interpretation of the references to colour in this figure legend, the reader is referred to the web version of this article.)

satellite observations, especially under cloudy skies. The general approach to infer surface longwave radiation is by means of some well-known parameterizations using field meteorological measurements as inputting data (Duarte et al., 2006; Kjaersgaard et al., 2007). Those calibrated parameterizations may be a very useful tool to estimate local surface longwave radiation where regular temperature, humidity and fractional cloud cover observations are available, but are incapable of capturing regional longwave radiative fluxes and characterizing the overall distribution patterns. Thus, this approach can not directly be adopted to map reliable watershed and regional NR. Another approach to obtain NR is through analyzing the relationship between net radiation and solar radiation to avoid the estimation of surface longwave fluxes (Alados et al., 2003; Hu et al., 2012; Kaminsky and Dubayah, 1997; Kustas et al., 1994). Since surface solar radiation can be estimated relatively accurately from satellite data, this relationship would have direct relevance for mapping regional net radiation. Though the relationship as well as its affecting factors had been widely explored in previous researches, we notice that its spatial dependence is very strong. In order to acquire complete NR maps under all sky conditions as surface SSR, we finally adopted this approach but re-developed this relationship using our surface radiation measurements.

The current study is placed in the Heihe river basin, a typical oasis-desert area in northwest China. But the study approach is conceived as a general method of estimating surface PAR, SSR and NR, which can be expediently revised and applied into other watersheds and regions. The Heihe river basin is one of the hottest research areas in China, and well known in the Chinese scientific community for the “Heihe Plan” launched by the National Natural Science Foundation of China and several large comprehensive experiments, including HEIFE, WATER and HiWATER (Chen et al., 2014; Hu et al., 1994; Li et al., 2013, 2009). Consequently, our case study not only promoted better understanding on regional estimations of surface radiation budget components based on the combination of satellite and surface data, but also provided surface PAR, SSR and NR products of different timescales for the various researches and applications over this watershed.

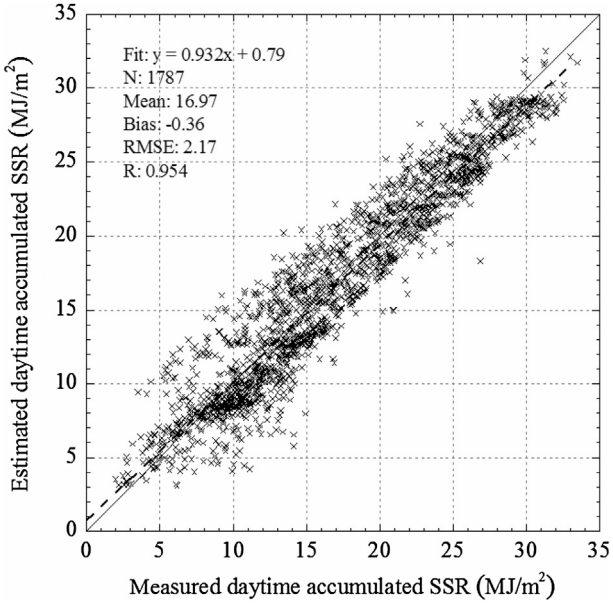

Fig. 5. Estimates of daytime accumulated SSR versus surface observed values. Solid and dash lines denote the 1-1 line and the fitted line, respectively.

2. Data preparation

Three groups of data were prepared in advance for the present study. Surface PAR and SSR retrievals rely on TOA reflectance and brightness temperature data from Geostationary Meteorological Satellite (GMS); surface NR estimation needs ground measurements to calibrate the relationship between net radiation and solar radiation; whereas some ancillary data on surface and atmospheric states are both required by the aforementioned two processes. In addition, another group of independent ground observation data was also prepared for validations.

2.1. GMS data and ground measurements

The Japanese GMS MTSAT2R (Multifunctional Transport Satellite) covering East Asia and West Pacific is utilized to retrieve instantaneous surface PAR and SSR. MTSAT2R can observe the Northern Hemisphere of the Earth every 30 min and has one visible and four infrared channels, in which VIS and IR1 channel will be used in our study.

Ground measurements were principally collected by two separated experiments, WATER and HiWATER over Heihe river basin (Li et al., 2013, 2009). Year 2008 or 2009 radiation measurements from five WATER sites are chosen to calibrate the relationship between net radiation and solar radiation, while observations from four WATER sites and four HiWATER sites in year 2012 are used for the final validations. Detailed information on these sites is listed in Table 1. The typical observation errors should not exceed 5% and inconsistency among different instruments approximately is within 3% (Xu et al., 2013).

2.2. Daily surface and atmospheric state parameters

Due to MTSAT2R sparse spectral channels, some surface and atmospheric state parameters affecting surface incident PAR, SSR and NR can not be determined just relying on MTSAT2R observations. These state parameters include surface snow cover, BRDF (Bidirectional Reflectance Distribution Function) albedo parameters, NDVI (Normalized Difference Vegetation Index), aerosol optical depth (AOD) and water vapor content (WVC) in atmosphere. Here we will use MODIS (Moderate Resolution Imaging Spectrometer) data to offset the deficiency of MTSAT2R observations. Namely, various MODIS products are utilized to obtain the above surface and atmospheric state parameters. MODIS products belong to polar-orbiting satellite products. Strictly speaking, their temporal resolution is too low to satisfy the demand of high temporal frequency surface radiation products. However, compared with cloud these parameters' fluctuation and influence on surface radiation both are relatively small. Therefore, in our study these parameters products were prepared on a daily timescale except AOD.

Fig. 1 gives the simplified flowchart on how to produce these parameters products. In view of the sparse aerosol retrievals over northwestern China, AOD estimates from MOD/MYD04 products would be separated according to season and elevation, and then clustered into two types to characterize the summer and winter half year average aerosol loading. Daily WVC would be extracted and averaged from MOD/MYD05 near-infrared total precipitable water Products, whereas daily NDVI was calculated by MOD/MYD09Q1 surface reflectance products. Based on MOD/MYD10A1 fractional snow cover products, we adopted the termed temporal and spatial filters to reduce and eliminate cloud coverage for daily snow cover and snow albedo (Parajka and Bloschl, 2008). Meanwhile, MCD43B1/B2 BRDF-Albedo model parameters products were used to obtain snow-free surface albedo at any solar zenith angle, and combining previous snow albedo we finally acquired the successive surface albedo products whether surface was covered by snow or not.

All these obtained parameters were rescaled into the daily products with 1 km resolution, and gaps among them would be filled through temporal or/and spatial interpolation approach which utilizes the neighboring information in time or/and space to compensate the invalid values.

3. Methodology

This section presents the framework to estimate surface PAR, SSR and NR under all sky conditions. An overview of instantaneous PAR and SSR retrievals is given first, followed by a detailed description on the estimation of instantaneous NR; while methods for hourly and daytime accumulated PAR, SSR and NR which are developed on the instantaneous products are simply summarized finally. Fig. 2 outlines the overall flowchart of the proposed methodology.

3.1. Instantaneous PAR and SSR retrievals

We still adopt the look-up Table (LUT) approach to directly retrieve instantaneous PAR and SSR from MTSAT2R TOA observations. But compared with our previous algorithm(Huang et al., 2011), the following improvements are imported: (1) the LUT is updated according to recent researches on representative aerosol and cloud optical properties; (2) cloud phase determination is tried in the new algorithm to desire more quality retrieval results.

3.1.1. Improved LUT

"Moderately Absorbing/Developing" aerosol optical model developed by Levy et al. (2007) and subsequently applied to the second generation MODIS standard dark-target aerosol algorithm, is selected here. The new aerosol model would be introduced into LibRadtran (Mayer and Kylling, 2005) to replace default aerosol models for radiative transfer modelling. Besides more appropriately characterizing aerosol absorption and scattering properties of atmosphere, this update also is beneficial to logically straightly utilize MODIS standard aerosol products in the algorithm.

Furthermore, the improved LUT increases the description on ice cloud bulk optical property. The ice cloud model of Baum et al.

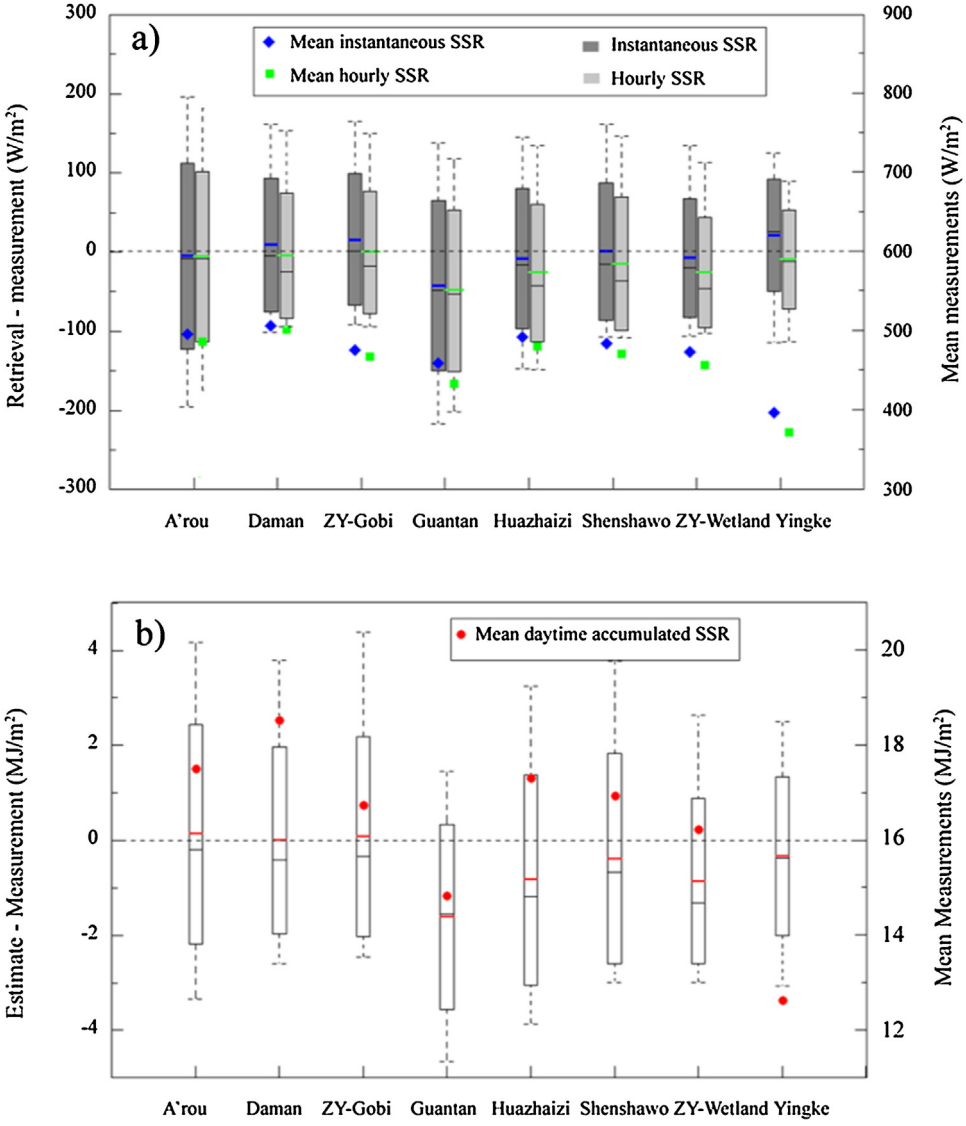

Fig. 6. Boxplot of errors between the retrieved and measured instantaneous and hourly SSR (a), and daytime accumulated SSR (b) at each site. The boxes denote 1 SD, and the whiskers extend from the 2.5th to the 97.5th percentile. Color short lines in boxes are mean errors, while black ones are median errors.

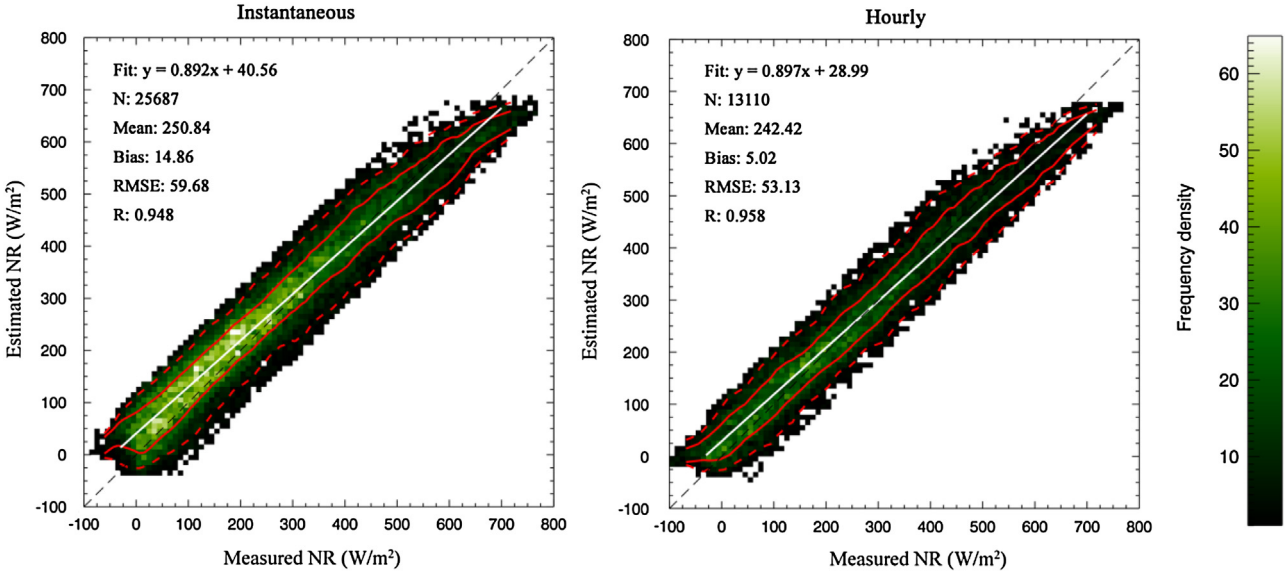

Fig. 7. Comparisons of the measured and estimated instantaneous (left) and hourly (right) surface NR. Please refer to Fig. 4 for the explanation of the symbols.

Table 1
Surface meteorological site information.

Site	Surface cover	Location	Experiment	Period
A'rou	Rangeland	100.46°E, 38.05°N	WATER	2008, 2012
Yingke	Farmland	100.41°E, 38.86°N	WATER	2008, 2012(Jan.–Mar.)
Huazhaizi	Desert	100.32°E, 38.77°N	WATER	2009, 2012
Maliantan	Grassland	100.28°E, 38.55°N	WATER	2008
Linze	Sparse vegetation	100.67°E, 39.25°N	WATER	2008(Jan.–Oct.)
Guantan	Forest	100.25°E, 38.53°N	WATER	2012(Jan.–Mar.)
Daman	Farmland	100.37°E, 38.86°N	HiWATER	2012
Zhangye Wetland	Wetland	100.45°E, 38.86°N	HiWATER	2012(Jun.–Dec.)
Zhangye Gobi	Gobi	100.30°E, 38.91°N	HiWATER	2012(May–Dec.)
Shenshawo	Desert	100.49°E, 38.79°N	HiWATER	2012(May–Dec.)

(2011) based on a habit mixture developed for midlatitude ice clouds, which also was used in MODIS standard cloud products (Yang et al., 2007), is adopted and considered as the typical ice cloud property over northwest China. In the LUT, an effective particle radius of 25 μm representing the peak of the global distribution of effective particle sizes (Meyer et al., 2007) is designated. Bigger size of ice crystals inevitably results into the stronger forward scattering peaks than water cloud (the effective particle radius is ~10 μm). Thus, in radiative transfer calculations the phase functions of ice cloud would be truncated, and expanded in terms of Legendre polynomials using the Delta-fit method (Hu et al., 2000). In a word, the new LUT greatly assimilated the recent efforts of MODIS science teams; while a detailed discussion on its creation cloud be found in other literatures (Huang et al., 2011; Liang et al., 2006).

3.1.2. Estimate MTSAT2R VIS surface reflectance

We expected using MTSAT2R visible TOA reflectance to diagnose and capture the changes of cloud fields in atmosphere (Huang et al., 2011). Towards this goal, MTSAT2R surface reflectance needs to be determined in advance.

Here minimum reflectance technique is adopted to estimate the MTSAT2R surface reflectance. Taking eight days as a time window, TOA reflectance time series was filtered to search for the minimum TOA reflectance. Generally speaking, TOA reflectance under cloudy skies is distinctly larger than that under clear skies, so the atmospheric condition of minimum TOA reflectance is inclined to be clear. Then atmospheric correction would be performed and surface reflectance in the time window was calculated. In homologous approaches, the underlying philosophy all is the surface reflectance changes little over short time intervals, while atmospheric states fluctuate wildly. Hence, if there were cases of snow cover partly existing in a time window, they would be dealt with separately in a similar way.

Nevertheless, there are still some extreme cases that all atmospheric conditions in the eight days are cloudy. Thereby, a temporal filter method is adopted to further analyze the time series of snow-free surface reflectance and reduce the cloud contaminations. Specifically, if one reflectance value in one time series of snow-free surface reflectance is larger than 0.4, we think it is very likely contaminated by cloud. Subsequently, this reflectance value is discarded and replaced by the interpolation from two adjacent reflectance (≦0.4).

3.1.3. PAR and SSR under all sky conditions

As mentioned earlier, we attempt to improve the LUT algorithm by discriminating the cloud thermodynamic phase. Currently, one of the advanced methods on cloud phase detection is MODIS bispectral infrared cloud phase algorithm, which combines 8.5 μm and 11.0 μm brightness temperature (Chylek et al., 2006; Platnick et al., 2003). Unfortunately, the MTSAT2R does not have 8.5 μm channel. Therefore, we adopt another widely used International Satellite Cloud Climatology Project (ISCCP) method to infer cloud phase (Rossow and Schiffer, 1999). ISCCP method is a kind of single channel thermal infrared threshold algorithm. In the study, MTSAT2R IR1 infrared channel (10.8 μm) brightness temperature is compared with the threshold value of 260 K to determine the cloud phase and lower brightness temperature is attributed to the ice cloud.

After surface reflectance is acquired, the atmospheric conditions can be directly inferred by comparing satellite TOA reflectance and the threshold reflectance of clear and cloudy skies. Here the cloud mask information is divided into three types (see Fig. 2), and labeled by:

$$\begin{cases} Clear: SR_i \le 1.2TR_{clear} \\ Undetermined: 1.2TR_{clear} < SR_i < TR_{cloudy} \\ Cloudy: SR_i \ge TR_{cloudy} \end{cases} \quad (1)$$

in which SR_i denotes anyone satellite TOA reflectance, TR_{clear} and TR_{cloudy} are the threshold reflectance of clear and cloudy, respectively. TR_{clear} was calculated using the ancillary aerosol optical depth from Section 2.2; while TR_{cloudy} supposed that the lowest optical depth of clouds was 3.

For the three different atmospheric conditions which are determined by Eq. (1) and presented in Fig. 2, different retrieving schemes are applied. For the "clear case", the direct and diffuse atmospheric flux transmittance (AFT) can be directly estimated by searching the gridded LUT parameters in accordance with the specific aerosol optical depth. For the "cloudy" case, satellite observing TOA reflectance and the simulated TOA reflectance at different cloud optical depth will be compared, and then the direct and diffuse AFT can be interpolated on the basis of the predefined AFT at different cloud optical depth. Whereas for the case of "undetermined", firstly satellite observing TOA reflectance needs to be compared with the simulated clear TOA reflectance (TR_{clear}) and the TOA reflectance (TR_{cloudy}) at the lowest cloud optical depth; subsequently the direct and diffuse AFT can be linearly interpolated according to the two corresponding AFT from the clear-sky and the lowest cloud optical depth. More detailed descriptions on this process can be found in our previous paper (Huang et al., 2011). Due to the total water vapor content in the LUT is assumed to 1.43 mm, we need to further adjust the transmittance of water vapor from a reference value to the actual value by a correction coefficient σ,

$$\sigma = T(WVC_i)/T\left(WVC_{ref}\right) \quad (2)$$

where $T(WVC_i)$ and $T(WVC_{ref})$ are the actual water vapor transmittance and the referenced water vapor transmittance, respectively. Incidentally, because in the spectral range of PAR (0.4–0.7 μm) there are basically not significant water vapor absorption bands, the transmittance of PAR does not need to be corrected. Namely, only SSR transmittance were corrected and water vapor transmittance was calculated using the parameterization scheme of Yang and Koike (2005). Owing to unreliable radiative transfer simula-

Table 2
Regression results for instantaneous net radiation versus net shortwave radiation.

Model[a]	$R_n = a(1-\alpha)R_s + b$		N	R^2[b]	SER[c]
	a	*b*			
Global	0.8293	−37.259	103491	0.9516	38.93
Stratified by weather condition					
Clear	0.8968	−76.7269	45823	0.9621	36.05
undetermined	0.8319	−19.1539	36225	0.9339	27.69
Cloudy	0.8214	−42.8184	21443	0.9379	40.27
Stratified by SZA					
SZA ≦ 45°	0.8199	−21.2837	31075	0.9552	44.92
SZA45–65°	0.7545	−20.0554	41353	0.935	32.24
Else SZA	0.6615	−25.8556	31063	0.797	29.27
Stratified by VSM					
VSM ≦ 0.1	0.7601	−31.1975	30727	0.898	32.49
VSM 0.1–0.25	0.8137	−34.7327	44927	0.9424	44.27
Else VSM	0.839	−30.9375	27837	0.9736	34.99
Stratified by Season					
Winter	0.7038	−25.4481	21371	0.8798	29.8
Spring	0.7798	−32.8134	28881	0.9661	33.37
Summer	0.8565	−35.8352	32227	0.9685	37.23
Autumn	0.8004	−26.245	21282	0.9297	40.27
Stratified by NDVI					
NDVI ≦ 0.2	0.7378	−37.1324	53278	0.9181	38.48
NDVI 0.2–0.5	0.7906	−30.4314	30415	0.9672	33.86
Else NDVI	0.8707	−28.7025	19798	0.9877	26.36

[a] Robust Least Trimmed Squares (LTS) regression analysis (number of observations that determine the LTS estimate is 95%N).
[b] Robust multiple R^2.
[c] Scale estimate of residuals.

Table 3
Self-validations for the different models.

Model	Bias	MRE (%)	RMSE
Global	0.83	15.4	41.47
Weather condition	−2.25	15.4	42.83
SZA	−0.73	14.1	40.31
VSM	−0.15	14.9	41.04
Season	−0.83	14.6	40.42
NDVI	−1.71	14.0	38.09

tions at large solar zenith angle (SZA), all retrievals demand SZA must be less than 80°.

3.2. Estimation of instantaneous NR

Many authors had investigated the feasibility of estimating net radiation from surface solar radiation which is more readily available from satellite data, and believed the simple linear regression was very successful (Alados et al., 2003; Kaminsky and Dubayah, 1997; Kustas et al., 1994). That is, net radiation R_n can be related to solar radiation R_s by means of,

$$R_n = a(1-\alpha)R_s + b \quad (3)$$

where α is the shortwave surface albedo and *a* and *b* are regression coefficients. Considering the empirical nature of the relationships between R_n and R_s, we used 2008 or 2009 year surface flux data from five WATER sites in Heihe river basin to recompute the regression coefficients and analyze their affecting factors.

Instantaneous regression relationships were established on the basis of 10-min surface measurements, and the affecting factors included weather condition, solar zenith angle, volumetric soil moisture (VSM), season and NDVI. Compared with the previous studies, NDVI is a new imported affecting factor. Here the robust least trimmed squares regression was adopted rather than the simple linear fit to reduce the possible influence from observational errors. Table 2 gives the final regression results and Table 3 presents the self-validations on the regression relationships.

Table 4
Regression results for hourly net radiation versus net solar radiation.

Model	$R_n = a(1-\alpha)R_s + b$		N	R^2	SER
	a	*b*			
Global	0.8276	−37.0133	17209	0.9498	38.40
NDVI ≦ 0.2	0.7314	−34.9224	8860	0.9149	38.08
NDVI0.2–0.5	0.7913	−31.5197	5057	0.9658	33.37
Else NDVI	0.8867	−27.7151	3292	0.9874	25.49

Table 5
Regression results for daytime accumulated net radiation versus net shortwave radiation.

Model	$R_n = a(1-\alpha)R_s + b$		N	R^2	SER
	a	*b*			
Global	0.7689	−0.8704	1700	0.9323	1.249
NDVI ≦ 0.2	0.6218	−0.7339	943	0.8717	1.211
NDVI0.2–0.5	0.7182	−0.2186	485	0.941	1.069
Else NDVI	0.7606	0.1344	272	0.9825	0.6042

It is very obvious that except weather condition the inclusions of other information all provide a slight improvement on the estimation of NR, but relatively the benefits of including NDVI are more outstanding. Coefficient of determination of as high as ~0.98 illustrates the fluctuation of surface NR basically can be completely explained by surface SSR. It seems that in a typical oasis-desert area such as Heihe river basin NDVI is a more important affecting factor for the relationships between net radiation and net solar radiation. Moreover, more fortunately the NDVI maps can be conveniently acquired by satellite data. Therefore, the NDVI dependent models in Table 2 finally were used to estimate instantaneous NR; while the surface albedo in Eq. (3) were calculated according to the BRDF-Albedo model parameters obtained in Section 2.2.

3.3. Hourly and daytime accumulated PAR, SSR and NR

As done by Deneke et al. (2008) and Huang et al. (2011), we still defined the temporal mean AFT as the ratio of integrated irradiances at the surface and TOA to calculate hourly and PAR and SSR. Namely, hourly mean AFT is the weighted average of three instantaneous AFT using μ_0 (cos(SZA)) as the weighting factor, instead of simple arithmetic mean. Whereas daytime accumulated PAR and SSR would be computed by the five-point Newton-Cotes integration method based on hourly PAR and SSR.

Meanwhile, relationships between net radiation and net solar radiation at hourly and daytime timescales were explored using the same methods as Section 3.2. Tables 4 and 5 show the regression results for hourly and daytime accumulated NR. Regular fluctuations of the regression coefficients *a* and *b* with stratified NDVI also suggest that the relationships have a strong dependence on NDVI, and regressions classified by NDVI value are appropriate. Note that in the paper instantaneous and hourly PAR, SSR and NR have units of W/m^2, while for the daytime accumulated the units are MJ/m^2.

4. Results

The aforementioned methodology was applied to Heihe river basin, northwest China to produce instantaneous, hourly and daytime accumulated PAR, SSR and NR products of year 2012, when and where many experimental researches were extensively and collectively carried out. In this section, the accuracies of these products were evaluated by comparisons with surface measurements.

4.1. Evaluation of PAR products

The PAR observation was only conducted at Daman site from HiWATER (see Table 1). Therefore, instantaneous PAR at 30-min resolution, hourly and daytime accumulated PAR were preliminarily evaluated using the measurements from this site, respectively. According to the researches of Deneke et al. (2009) and Huang et al. (2016), for more reasonably validating instantaneous satellite estimates of surface irradiance, the surface measurements of 10 min would be averaged into 40 min to increase spatial representativeness of ground-based point observation. Raw satellite retrieved products had been smoothed using 5×5 spatial windows (about $5 \times 5\,km^2$) to reduce 3D radiative effects caused by clouds.

The error histogram and the summaries (e.g., bias, R^2 and RMSE) on the instantaneous, hourly and daytime accumulated evalutions are shown in Fig. 3. In the figure, the error bin size for instantaneous and hourly evaluations both is $5\,W/m^2$, and for daytime accumulated evaluation, it is $0.2\,MJ/m^2$. From the summary on the instantaneous evaluation, we found that fairly accurate surface PAR retrievals had been produced, but slight overestimation (~6% of mean value) was visible. Consequently, appreciable overestimations would also appear in hourly and daytime accumulated products because these products were produced based on the instantaneous retrievals. Nevertheless, overall the accuracies here are comparable with the results reported by other researches (Liang et al., 2006), and our method is able to considerably successfully estimate surface PAR from instantaneous to hourly, to daytime.

4.2. Evaluation of SSR products

Pyranometer measurements collected by WATER and HiWATER at eight sites in Heihe river basin were used to validate the accuracy of SSR retrievals. As the evaluations of PAR products, SSR evaluations were conducted on three different timescales, and for the instantaneous evaluation similar processes on the measurements and retrievals were done, too.

Fig. 4 is a couple of frequency scatterplots. The left is the instantaneous comparisons of total retrieved SSR at these eight sites, and the right is the hourly comparisons. In the figure data are sorted according to the ordered pairs (measurement, retrieval) of SSR in $10\,W/m^2$ intervals, so the gradual color represents the number density falling into each interval grid. The white and black dash lines are the fitted line and the 1-1 line, respectively; while two red solid lines and two red dash lines respectively enclose 66% and 95% of retrievals. Statistics of the comparison results are also summarized and presented in the top left corner of the figure. Correlation coefficients of as high as 0.94, $\sim 90\,W/m^2$ of RMSE, and $-0.58\,W/m^2$ of bias reveal that a very good agreement between the retrieved and measured SSR can be expected for instantaneous products. Despite greater deviation of the bias, the higher correlation coefficient and the lower RMSE both indicate that hourly SSR products on the whole are better than instantaneous products. In addition, one noticeable feature demonstrated by Fig. 4 is the retrieved results will change from overestimation into underestimation as measured SSR increases (the horizontal axis). Possible explanations for this behavior will be discussed in Section 5.

Next, the evaluation of daytime accumulated SSR products is shown in Fig. 5. The RMSE of $2.17\,MJ/m^2$, which is ≈12% of the mean value, is far less than that found in instantaneous or hourly products (both >18%). This suggests that daytime accumulated SSR products have higher accuracy than instantaneous or hourly products. One of the possible reasons is the underestimation in certain high value range and the overestimation in certain low value range may be offset on daytime scale. A distinctly higher correlation coefficient further confirms this conclusion. Moreover, a bias of $-0.36\,MJ/m^2$, about −2% of the mean value, indicates that estimation of daytime accumulated SSR is basically unbiased.

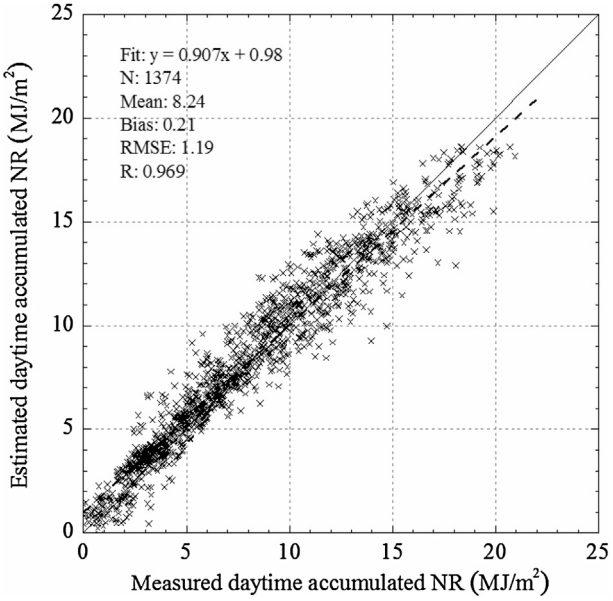

Fig. 8. Estimates of daytime accumulated SSR versus surface observed values. Solid and dash lines denote the 1-1 line and the fitted line, respectively.

Site by site evaluations on SSR products were also performed, and error boxplot of Fig. 6 provides the visual assessments at each site. Instantaneous and hourly evaluations are displayed together in the top; while daytime accumulated evaluation is shown in the bottom due to their different unit. The figure is designed into having two different *y* axes to facilitate that one can simultaneously see the distribution of the absolute error and relative errors comparing with averaged measurements. The boxes and whiskers denote 66% (~1 standard deviation) and 95% (~2 standard deviation) intervals of differences between retrieved and measured SSR, respectively. Though most of the sites compare well as expected, clear underestimation can be seen at Guantan site. Since this site only has measurements from Jan. to Mar., more cases of snow cover are expected (7.1% vs. averaged 5.7%). And in Section 5 we will see that snow cover will result in SSR is heavily underestimated. Nevertheless, underestimation caused by snow cover still is not enough to account for such large a deviation. Guantan site locates in a canyon, and its surrounding terrain is very complex. Another possible explanation is the surface reflectance is underestimated due to the presence of surface shadows, and consequently the underestimations of atmospheric flux transmittance and SSR are produced in succession.

4.3. Evaluation of NR products

Similar frequency scatterplots on instantaneous and hourly NR are displayed in Fig. 7, respectively. But here only six sites' measurements are used, and A'rou and Guantan are excluded because their measurements of longwave radiation are very suspicious. As in Fig. 4, the color of each ordered pair (10×10 increment) represents the number density of such matchups. Red solid lines and red dash lines respectively represent 66th and 95th percentiles. Meanwhile, Fig. 8 shows the evaluation of daytime accumulated NR products.

Quality statistics (R, Bias and RMSE) presented in the figures demonstrate that the estimated NR have statistically significant correlation with surface observed NR, and further indicate a very good agreement between them. Since the NR are estimated using

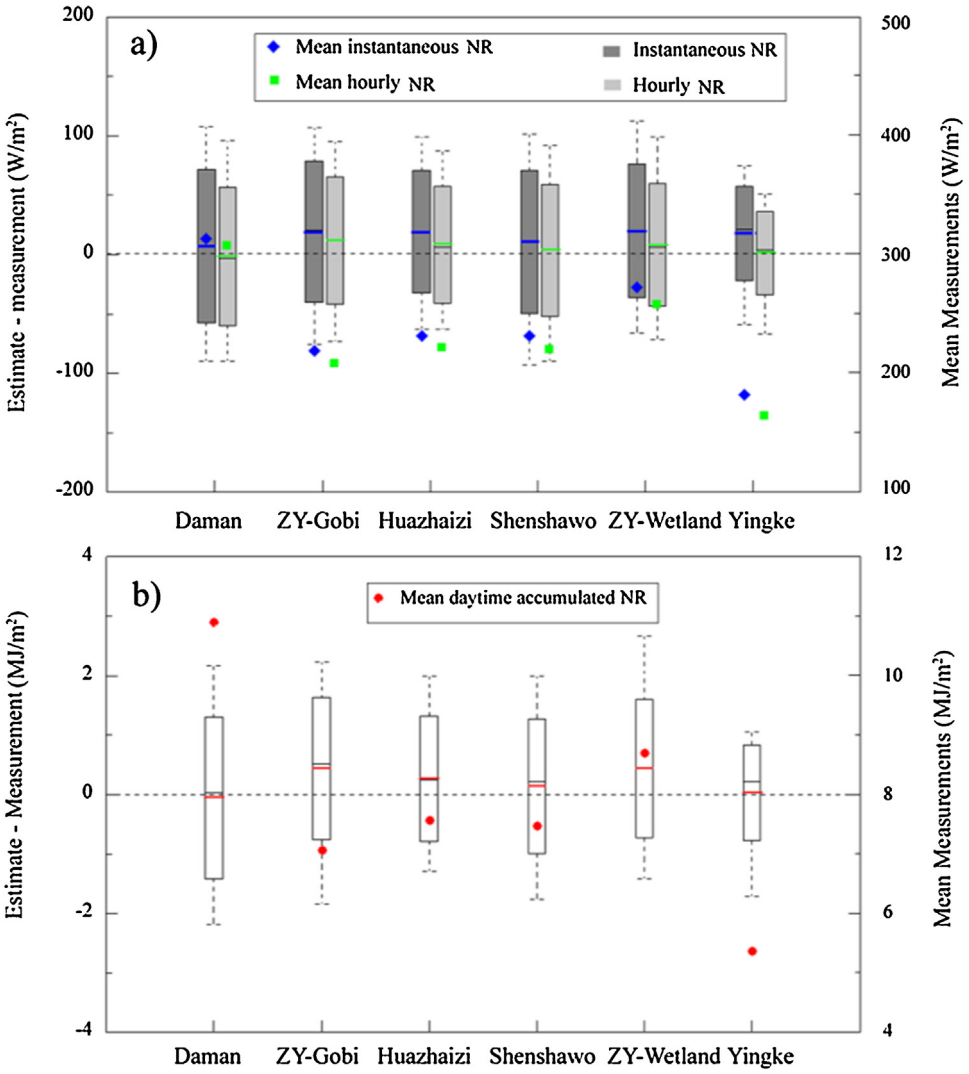

Fig. 9. Boxplot of errors between the measured and retrieved instantaneous and hourly SSR (a), and daytime accumulated NR (b) at each site. Please refer to Fig. 6 for the explanation of the symbols.

the SSR retrieved from satellite data, it may include a comparable error characteristic like SSR. That is, the underestimation for high NR values and the overestimation for low NR values. However, from these figures we find that the degree of underestimation or overestimation has significantly become smaller in comparison to SSR. In addition, another feature can be also easily recognizable. Accuracy of hourly NR products is clearly higher than that of instantaneous NR products; while relative RMSR of 11.7% of daytime accumulated NR indicates that daytime accumulated NR products are obviously better than hourly NR products, which have a relative RMSR of 21.7%.

Fig. 9 gives the error boxplots of NR products by individual site. As opposed to being slightly underestimated at most sites for SSR products, to a certain extent NR products are overestimated at most sites, especially for instantaneous products. Appreciable bad performance at Zhangye Gobi and Wetland is because the relationship between NR and net shortwave radiation developed by us does not use the data from gobi and wetland surface cover.

5. Discussion

As mentioned in Section 4, instantaneous and hourly products show a systematic error that surface radiation components are appreciably overestimated in the lowest quarter of the range, but are underestimated in the highest quarter of the range. In order to analyze the potential causes, accuracies of instantaneous products are further explored according to different atmospheric conditions (see Section 3.1.3). Fig. 10 depicts instantaneous PAR, SSR and NR error frequency distribution under the three atmospheric conditions. For PAR and SSR, it is clear that under clear atmospheric condition the values are obviously underestimated, on the contrary under cloudy condition significant overestimation appears, and under "undetermined" condition the evident deviation does not exist. However, analogous trends are not apparent in NR products. It seems that, to a considerable extent, this systematic error would be rectified in the process of estimating NR.

Similar systematic error also can be seen in other literatures (Deneke et al., 2008; Huang et al., 2013), though the amplitudes of overestimation or underestimation may be lower than those presented here. For the underestimation trend under clear condition, we further analyze the MODIS aerosol products and surface SSR measured data. Using available AOD surface measurements from Jun. to Sep. in year 2012 over Heihe river basin, we find that the AOD overall is overestimated ~0.04. While, the analysis of measured data shows that ~0.7% of SSR seem to be too high, even higher than corresponding TOA solar irradiance. These exorbitant mea-

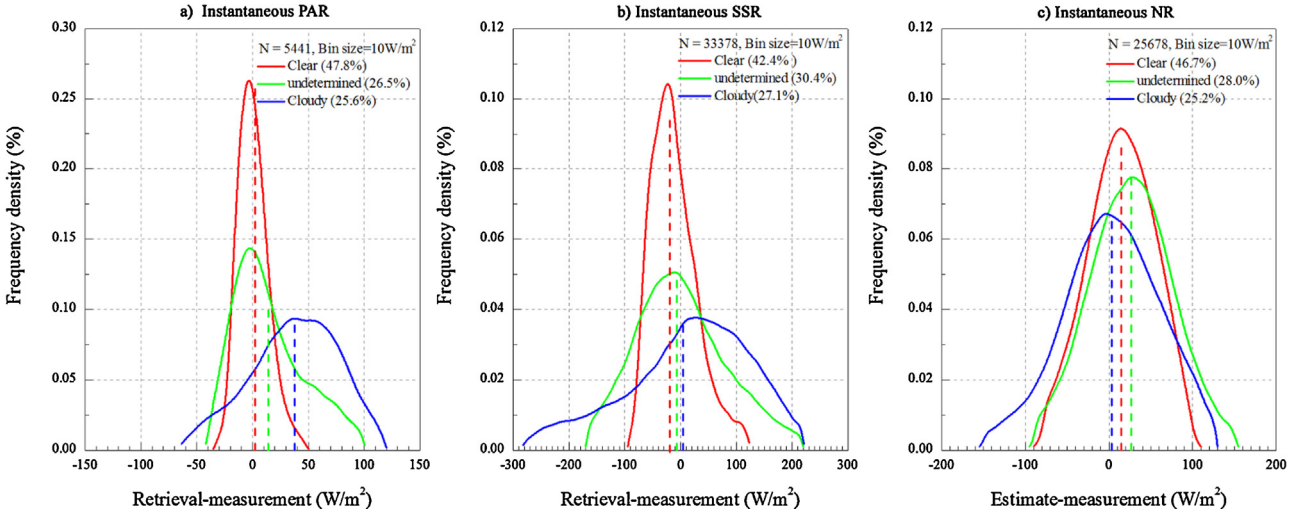

Fig. 10. Error frequency distribution of the surface instantaneous PAR (a), SSR (b) and NR (c) under different atmospheric conditions. Dash lines denote the means of the corresponding errors.

surements may be caused by horizontal photon transport nearby clouds in atmosphere or extra radiation reflected by surrounding terrain. For the overestimation trend under cloudy condition, one possible reason is satellite observing TOA reflectance has saturated for too thick clouds, subsequently can not reflect the change of cloud optical depth, and result in overestimated atmospheric transmittance.

Another systematic error originates the effects of snow cover. Table 6 lists these products' distinct accuracy performances over snow cover or not. Obviously, compared with the snow-free surface condition, the accuracies of various products over snow cover will dramatically drop and a systematic underestimation is found, especially for SSR products. In presence of snow, the surface radiative field will become anomalously complicated, and unordered reflectanced and scattered light may extremely reinforce surface actual incident radiation, especially under cloudy skies. Meanwhile, the minimum reflectance technique adopted by us also is apt to underestimate surface reflectance for varying snow cover proportions in a time window, and subsequently lower atmospheric transmittance and surface incident irradiance are caused. Currently, estimation of surface radiation components over snow cover still is a very challenging task (Pinker et al., 2007).

Besides, an interesting phenomenon is the accuracies of all products have significant improvements with incremental timescales. The fact that cloud inhomogeneity and 3D radiative effects in satellite-based radiation products can be appreciably reduced and spatial representativeness of surface measured data can be appreciably increased through simply temporally averaging, has been widely accepted (Huang et al., 2016). Meanwhile, upscaling temporal resolution also can make some systematic errors be offset, and more quality products are expected.

In principle, cloud phase determination would lead to a significant improvement of PAR and SSR retrievals because ice clouds and water clouds have rather different optical properties. However, disappointingly a better performance was not found when the cloud phase was identified by the simple thermal infrared threshold algorithm, and even a greater degree of overestimation is seen. This finding is consistent with the study of Deneke et al. (2005) based on Advanced Very High Resolution Radiometer (AVHRR) data. Wolters et al. (2008) evaluated the ISCCP-like cloud phase determination method and pointed out that for thick water and ice cloud the instantaneous bias was within 5%, while for pure water cloud it was ~10%. Therefore, the possible reasons and improvements need a more in-depth investigation, which is beyond the scope of the current study.

6. Conclusions

Sophisticated agricultural, hydrological and meteorological applications on a catchment or regional scale need high quality surface radiation as inputs, which are not able to be provided by the present radiation products. Thereby, in this paper a methodology to obtain quality PAR, SSR and NR under all sky conditions by exploiting the synergy of multi-source data, is proposed.

Towards this goal, the LUT algorithm of Huang et al. (2011) was improved to retrieve PAR and SSR, and the new NDVI dependent relationships between net radiation and solar radiation were developed to estimate NR. In order to get the correct representation of aerosol and cloud optical properties, the latest research achievements from MODIS science team were assimilated a lot into radiative transfer model. In essence, the new PAR and SSR retrieving algorithm utilizes dual channels' data of MTSAT (VIS and IR1) instead of previous single channel to capture fluctuating cloud information; whereas the new relationships between net radiation and solar radiation are fitted by using NDVI as an indicator to characterize different surface longwave radiation balance features. The proposed methodology was applied to Heihe river basin and products on three different timescales were produced due to their common use. Then, accuracies of these products were quantified using the surface measurements from WATER and HiWATER.

Through our study, the following conclusions can be drawn: (1) The proposed methodology can give high quality surface radiation products. Evaluations over Heihe river basin confirm that the produced products have an extremely good agreement with surface measurements. (2) Though inclusions of other information can also slightly improve the relationships between net radiation and solar radiation, importing NDVI to classify the relationships performs best in Heihe river basin. (3) In PAR and SSR products, there are a systematic underestimation in certain high value range and a systematic overestimation in certain low value range, while in NR products these systematic errors may be significantly reduced. (4) In presence of snow cover, the accuracy of products will distinctly decline and a systematic underestimation is found, especially for SSR products. (5) To an extent, the accuracies of all products will be improved with ascending timescales. That is, daytime accumulated products outperform hourly products, and hourly products are better than instantaneous products. (6) Distinguishing cloud phase by

Table 6
Summary statistics on accuracies of the various products over two different surface conditions (snow cover or not).

Products	Land/Snow (N)	Bias(W/m^2, or MJ/m^2)[a]	RMSE(W/m^2, or MJ/m^2)	Robust linear regression		
				a	b	r
Ins PAR	Land (5239)	13.66	38.38	0.886	34.77	0.97
	Snow (182)	−0.66	37.81	0.655	37.14	0.79
Hur PAR	Land (2616)	13.22	35.60	0.884	34.82	0.97
	Snow (104)	−0.45	34.10	0.700	29.58	0.84
Daytime PAR	Land (269)	0.587	1.03	0.929	1.06	0.97
	Snow (14)	0.232	1.22	0.818	0.81	0.59
Ins SSR	Land (31435)	2.83	90.11	0.864	68.13	0.97
	Snow (1943)	−50.73	122.11	0.725	50.87	0.82
Hur SSR	Land (15993)	−12.21	85.77	0.877	44.83	0.97
	Snow (1055)	−49.82	121.89	0.725	42.30	0.85
Daytime SSR	Land (1661)	−0.26	2.07	0.944	0.61	0.97
	Snow (126)	−1.75	3.22	0.854	−0.02	0.80
Ins NR	Land (24501)	16.54	60.23	0.877	47.31	0.97
	Snow (1186)	−16.92	46.99	0.708	1.44	0.80
Hur NR	Land (12451)	6.27	53.59	0.884	34.36	0.97
	Snow (659)	−15.59	43.45	0.689	1.53	0.82
Daytime NR	Land (1293)	0.23	1.21	0.915	0.95	0.98
	Snow (81)	−0.08	0.89	0.740	0.31	0.83

[a] For instantaneous and hourly products, the unit is W/m^2; while for daytime accumulated products the unit is MJ/m^2.

the simple ISCCP thermal infrared threshold algorithm does not lead to any significant improvement of the PAR and SSR retrieval quality. The possible explanations on all these systematic errors have been discussed in Section 5. Whereas, the fact presented in the sixth item needs a more in-depth investigation.

Last, the resulting high resolution PAR, SSR and NR products as well as daily surface and atmospheric state parameters products provide primary driving data for regional energy, hydrologic and ecological processes, and will benefit the various studies that have been conducted or are about to be conducted in this region. These products are readily available on the web of WestDC (URL: http://westdc.westgis.ac.cn/data).

Acknowledgement

The authors would like to thank the MODIS science team and the LibRadtran developing team for their warm-hearted helps. This work was jointly supported by the National Natural Science Foundation of China (Grant: 91125004, 41471358 and 41571358), the Chinese Academy of Sciences Action Plan for West Development Program Project–"Remote Sensing Data Products in the Heihe River Basin: Algorithm Development, Data Products Generation and Application Experiments" (Grant: KZCX2-XB3-15), the interdisciplinary Innovation Team of the Chinese Academy of Science, and the One Hundred Person Project of the Chinese Academy of Sciences (Grant: 29Y127D01).

References

Alados, I., Foyo-Moreno, I., Olmo, F.J., Alados-Arboledas, L., 2003. Relationship between net radiation and solar radiation for semi-arid shrub-land. Agric. Forest Meteorol. 116 (3–4), 221–227.
Baum, B.A., et al., 2011. Improvements in shortwave bulk scattering and absorption models for the remote sensing of ice clouds. J. Appl. Meteorol. Climatol. 50 (5), 1037–1056.
Chen, G.D., et al., 2014. Integrated study of the water-ecosystem-economy in the Heihe river basin. Natl. Sci. Rev. 1 (3), 413–428.
Chylek, P., et al., 2006. Comparison of near-infrared and thermal infrared cloud phase detections. J. Geophys. Res. Atmos. 111 (D20).
Deneke, H., Feijt, A., van Lammeren, A., Simmer, C., 2005. Validation of a physical retrieval scheme of solar surface irradiances from narrowband satellite radiances. J. Appl. Meteorol. 44 (9), 1453–1466.
Deneke, H.M., Feijt, A.J., Roebeling, R.A., 2008. Estimating surface solar irradiance from METEOSAT SEVIRI-derived cloud properties. Remote Sens. Environ. 112 (6), 3131–3141.
Deneke, H.M., Knap, W.H., Simmer, C., 2009. Multiresolution analysis of the temporal variance and correlation of transmittance and reflectance of an atmospheric column. J. Geophys. Res. Atmos. 114.
Duarte, H.F., Dias, N.L., Maggiotto, S.R., 2006. Assessing daytime downward longwave radiation estimates for clear and cloudy skies in Southern Brazil. Agric. Forest Meteorol. 139 (3–4), 171–181.
Grant, R.H., Hollinger, S.E., Hubbard, K.G., Hoogenboom, G., Vanderlip, R.L., 2004. Ability to predict daily solar radiation values from interpolated climate records for use in crop simulation models. Agric. Forest Meteorol. 127 (1–2), 65–75.
Hu, Y.Q., et al., 1994. Some achievements in scientific research during HEIFE. Pleteau Meteorol. 13 (8), 225–236 (in Chinese).
Hu, Y.X., et al., 2000. Delta-fit: a fast and accurate treatment of particle scattering phase functions with weighted singular-value decomposition least-squares fitting. J. Quant. Spectrosc. Radiat. Transfer 65 (4), 681–690.
Hu, B., Wang, Y.S., Liu, G.R., 2012. Relationship between net radiation and broadband solar radiation in the Tibetan Plateau. Adv. Atmos. Sci. 29 (1), 135–143.
Huang, G.H., Ma, M.G., Liang, S.L., Liu, S.M., Li, X., 2011. A LUT-based approach to estimate surface solar irradiance by combining MODIS and MTSAT data. J. Geophys. Res. Atmos. 116.
Huang, G.H., et al., 2013. Preliminary validation of GLASS-DSSR products using surface measurements collected in arid and semi-arid regions of China. Int. J. Digital Earth 6, 50–68.
Huang, G.H., et al., 2016. Representativeness errors of point-scale ground-based solar radiation measurements in the validation of remote sensing products. Remote Sens. Environ., http://dx.doi.org/10.1016/j.rse.2016.04.001, in press.
Kaminsky, K.Z., Dubayah, R., 1997. Estimation of surface net radiation in the boreal forest and northern prairie from shortwave flux measurements. J. Geophys. Res. Atmos. 102 (D24), 29707–29716.
Kjaersgaard, J.H., Plauborg, F.L., Hansen, S., 2007. Comparison of models for calculating daytime long-wave irradiance using long term data set. Agric. Forest Meteorol. 143 (1–2), 49–63.
Kustas, W.P., Pinker, R.T., Schmugge, T.J., Humes, K.S., 1994. Daytime net-Radiation estimated for a semiarid rangeland basin from remotely-sensed data. Agric. Forest Meteorol. 71 (3–4), 337–357.
Levy, R.C., Remer, L.A., Dubovik, O., 2007. Global aerosol optical properties and application to Moderate Resolution Imaging Spectroradiometer aerosol retrieval over land. J. Geophys. Res. Atmos. 112 (D13).
Li, X., Pinker, R.T., Wonsick, M.M., Ma, Y.T., 2007. Toward improved satellite estimates of short-wave radiative fluxes Focus on cloud detection over snow: 1. Methodology. J. Geophys. Res. Atmos. 112 (D7).
Li, X., et al., 2009. Watershed allied telemetry experimental research. J. Geophys. Res. Atmos. 114.
Li, X., et al., 2013. Heihe watershed allied telemetry experimental research (HiWATER): scientific objectives and experimental design. Bull. Am. Meteorol. Soc. 94 (8), 1145–1160.
Liang, S.L., et al., 2006. Estimation of incident photosynthetically active radiation from Moderate Resolution Imaging Spectrometer data. J. Geophys. Res. Atmos. 111 (D15).
Liang, S.L., et al., 2013. A long-term global Land surface satellite (GLASS) data-set for environmental studies. Int. J. Digital Earth 6, 5–33.
Liu, R.G., Liang, S.L., He, H.L., Liu, J.Y., Zheng, T., 2008. Mapping incident photosynthetically active radiation from MODIS data over China. Remote Sens. Environ. 112 (3), 998–1009.
Lu, N., Liu, R.G., Liu, J.Y., Liang, S.L., 2010. An algorithm for estimating downward shortwave radiation from GMS 5 visible imagery and its evaluation over China. J. Geophys. Res. Atmos. 115.
Mayer, B., Kylling, A., 2005. Technical note: the libradtran software package for radiative transfer calculations–description and examples of use. Atmos. Chem. Phys. 5, 1855–1877.

Meyer, K., Yang, P., Gao, B.C., 2007. Ice cloud optical depth from MODIS cirrus reflectance. Ieee Geosci. Remote Sens. Lett. 4 (3), 471–474.
Parajka, J., Bloschl, G., 2008. Spatio-temporal combination of MODIS Images—potential for snow cover mapping. Water Resour. Res. 44 (3).
Pinker, R.T., Li, X., Meng, W., Yegorova, E.A., 2007. Toward improved satellite estimates of short-wave radiative fluxes—focus on cloud detection over snow: 2. Results. J. Geophys. Res. Atmos. 112 (D9).
Platnick, S., et al., 2003. The MODIS cloud products: algorithms and examples from Terra. Ieee Trans. Geosci. Remote Sens. 41 (2), 459–473.
Qin, J., Chen, Z.Q., Yang, K., Liang, S.L., Tang, W.J., 2011. Estimation of monthly-mean daily global solar radiation based on MODIS and TRMM products. Appl. Energ. 88 (7), 2480–2489.
Rossow, W.B., Schiffer, R.A., 1999. Advances in understanding clouds from ISCCP. Bull. Am. Meteorol. Soc. 80 (11), 2261–2287.
Trnka, M., Zalud, Z., Eitzinger, J., Dubrovsky, M., 2005. Global solar radiation in Central European lowlands estimated by various empirical formulae. Agric. Forest Meteorol. 131 (1-2), 54–76.
Wielicki, B.A., et al., 1996. Clouds and the earth's radiant energy system (CERES): an earth observing system experiment. Bull. Am. Meteorol. Soc. 77 (5), 853–868.
Wolters, E.L.A., Roebeling, R.A., Feijt, A.J., 2008. Evaluation of cloud-phase retrieval methods for SEVIRI on Meteosat-8 using ground-based lidar and cloud radar data. J. Appl. Meteorol. Climatol. 47 (6), 1723–1738.
Xu, Z.W., et al., 2013. Intercomparison of surface energy flux measurement systems used during the HiWATER-MUSOEXE. J. Geophys. Res. Atmos. 118 (23), 13140–13157.
Yang, K., Koike, T., 2005. A general model to estimate hourly and daily solar radiation for hydrological studies. Water Resour. Res. 41 (10).
Yang, P., et al., 2007. Differences between collection 4 and 5 MODIS ice cloud optical/microphysical products and their impact on radiative forcing simulations. Ieee Trans. Geosci. Remote Sens. 45 (9), 2886–2899.
Zhang, Y.C., Rossow, W.B., Lacis, A.A., Oinas, V., Mishchenko, M.I., 2004. Calculation of radiative fluxes from the surface to top of atmosphere based on ISCCP and other global data sets: refinements of the radiative transfer model and the input data. J. Geophys. Res. Atmos. 109 (D19).
Zhang, Y.C., Rossow, W.B., Stackhouse, P.W., 2006. Comparison of different global information sources used in surface radiative flux calculation: radiative properties of the near-surface atmosphere. J. Geophys. Res. Atmos. 111 (D13).
Zhang, T.P., Stackhouse, P.W., Gupta, S.K., Cox, S.J., Mikovitz, J.C., 2013. The NASA GEWEX surface radiation budget project: dataset validation and climatic signal identification. Radiat. Process. Atmos. Ocean (Irs2012) 1531, 636–639.
Zheng, T., Liang, S.L., Wang, K.C., 2008. Estimation of incident photosynthetically active radiation from GOES visible imagery. J. Appl. Meteorol. Climatol. 47 (3), 853–868.